

Electro-Powerless Balloon Soft Actuator with Manually Driven Fluidic Circuit

Ryosuke Matsuda, Zihao Song, and Hiroki Ota*

Balloon-type actuators have attracted scientific attention because they allow easy control of the output intensity and a high degree-of-freedom regarding shape and movement. However, they require bulky external pumps and electric power suppliers. This makes miniaturization and wearable device fabrication difficult. Herein, a balloon soft actuator that does not require a pneumatic pump or electric power supplier, and that uses a finger-operated pump based on a fluidic circuit and catalytic reaction, is proposed. This device can be driven without electric power multiple times by applying a vent valve system to exhaust the generated gas. Further, it is applied to two different types of applications—soft robots and wearable devices—by optimizing their structure and material. In conclusion, the proposed device is expected to lead to the development of a broad range of soft actuators for stand-alone robots and wearable devices in the future.

1. Introduction

In recent years, considerable research has been conducted on the fabrication of flexible and stretchable actuators. These actuators are based on soft materials used as basal substrates, such as magnetic-responsive materials^[1–3] and thermo-responsive gels,^[4–6] liquid metals,^[7,8] and flexible resins with piezoelectric properties.^[9] Among these actuators, balloon-type actuators driven by pumping have been proposed for a variety of applications, including walking robots,^[10] robot arms for grasping objects,^[11] and rehabilitation devices that can be worn on the hands to support hand movements of disabled people.^[12] Balloon-type actuators can be driven by a rubber seal material in an arbitrary shape that changes by pumping gas or liquid into the device. The advantage of this type of actuator is that

it can produce various strength outputs, molding flexibility, and different material selection.

While these balloon actuators have various advantages, it has been a challenge to make the entire system flexible and compact because the pumps are rigid, bulky, and transport a large amount of air to drive the balloon. Recently, a new system was proposed to drive a balloon actuator by generating gas through a chemical reaction in the device without direct air transport. This system uses a liquid as “fuel,” breaks it down into gas based on a chemical reaction, and drives balloons by using the volume difference between liquid and gas. This makes it possible to obtain the energy required to drive the actuator from

a small amount of liquid without requiring a large amount of electric power. However, this does not eliminate the need for a pump.

To solve this problem, several balloon actuators that do not require pumps have been proposed, such as those that vaporize organic solvents by heat, and those that directly infuse liquids by voltage. These are new systems that can infuse fluids or generate gases without a pump, and can achieve the same effect as pumping fluids without a pump. Although these methods successfully reduce pumps, all of these systems require a stable external electric power source. To solve these problems, finger pumps have been proposed as a method that does not require a power supply or external pump.^[13–15] Finger pumps transfer liquids by repeatedly pushing and releasing with a finger, and are mainly used for transferring and mixing liquids. However, it is difficult for such pumps to transfer large amounts of liquid, and the current limit of infusion volume is μL -sub- mL , making it difficult to drive large actuators.

In this study, we fabricated an infusion system by using a hand pump with a fluidic system, and demonstrated the implementation of a soft actuator that does not require external electric power, and is manually driven by gas generation based on a chemical reaction. In this mechanism, a hydrogen peroxide solution is infused by using a finger pump, and the liquid reacts with manganese dioxide as a catalyst to generate oxygen. Subsequently, the generated gas is used to inflate the balloon and obtain the driving force. A porous resin is used in the chemical reaction chamber to increase the contact area between the liquid and catalyst to improve the reaction efficiency. Additionally, a release valve was created inside the actuator to enable repetitive motion. The whole device with multiple types of functional components can be fabricated with a single 3D printing

R. Matsuda, Z. Song
Department of Mechanical Engineering
Yokohama National University
79-5 Tokiwadai, Hodogaya-ku, Yokohama, Kanagawa 240-8501, Japan
H. Ota
Graduate School of System Integration
Yokohama National University
79-5 Tokiwadai, Hodogaya-ku, Yokohama, Kanagawa 240-8501, Japan
E-mail: ota-hiroki-xm@ynu.ac.jp

 The ORCID identification number(s) for the author(s) of this article can be found under <https://doi.org/10.1002/aelm.202201065>.

© 2022 The Authors. Advanced Electronic Materials published by Wiley-VCH GmbH. This is an open access article under the terms of the Creative Commons Attribution License, which permits use, distribution and reproduction in any medium, provided the original work is properly cited.

DOI: 10.1002/aelm.202201065

process. This enables devices to be integrated, which previously had to be fabricated by integrating other technologies such as lithography. Based on this mechanism, a tentacle-inspired, soft gripper robot, and a grasp-assisting wearable device were fabricated.

2. Results and Discussion

Images of the fabricated device are shown in **Figure 1**; and Video S1 (Supporting Information). The device could expand and shrink multiple times through liquid decomposition and gas leakage. Figure 1i–iv shows the driving system of the device. This device contains a tank, pump, diode, reaction area, vent valve, and actuation part (Figure 1i). The device can be driven by pushing the pump with a finger. The pump can allow the flow of liquid in the forward direction, and the diode prevents backward flow. In this case, hydrogen peroxide was decomposed into oxygen by contacting manganese dioxide inside the porous structure of urethane resin (Figure 1ii). The porous structure can increase the contact area and reaction efficiency. Subsequently, the generated oxygen expands the balloon actuator tip of the device. The diode system can prevent gas back-flow (Figure 1iii). Oxygen gas can then be leaked by opening the vent valve (Figure 1iv). This valve can be opened by a finger, as well as the pump drive.

The structure of the device is illustrated in **Figure 2A**. The device was constructed by using a tank, diode, pump, reaction sponge, balloon, and vent valve. This functionality was achieved by using a three-layered structure which included the pump, diode, and chemical reaction layers. In addition, as shown in Figure 2A; and Figure S1 (Supporting Information), the pumping layer was composed of two types of silicone resin with different hardness values. By attaining a difference in the hardness between the actuator and infusion/reaction part, the expansion caused by the gas can be concentrated at the balloon actuator part.

In this device, a mixture of KE-01603 (hard silicone) and Ecoflex 00–30 (soft silicone) is used for the mechanical part, and only Ecoflex 00–30 is used for the balloon part (Figure S1,

Supporting Information). As shown in Figure S1 (Supporting Information), Ecoflex is a very soft and stretchable silicone resin and can stretch up to ≈ 6 times. There are several types of Ecoflex, such as numbered 00–10, 00–50, depending on their mechanical properties. The smaller-numbered Ecoflex resins deformed plastically, whereas the larger numbered Ecoflex resins were stiffer and required more force to deform. With Ecoflex 00–10, 00–30, and 00–50, the force required to stretch the resin to twice its initial length was measured, and the length after released was measured (Table S1, Supporting Information). As can be seen from the table, the 00–10 balloon has a large plastic deformation after release, which may affect repeated balloon stretching. The plastic deformation of the 00–50 balloon is small, but the force required to stretch the balloon is more than twice that of the 00–30 balloon. This implies that the internal pressure increases when the balloon is inflated; this might damage components other than the balloon actuator (e.g., the diode and the hermeticity of the outer circumference). Considering both these factors, 00–30 was selected for the device material. However, if diode function is improved and pressure resistance is further enhanced, a harder resin such as 00–50, which does not cause plastic deformation, could be used for more stable and repeated operation.

Furthermore, Ecoflex has been reported to swell and change its properties in organic solvents,^[16] and its chemical resistance to organic solvents is considered low. Silicone is reported to have high chemical resistance to hydrogen peroxide.^[17] A chemical-resistance test is not necessary when this device is operated without organic solvents.

This device uses a system for pumping liquids without external power (Figure 2B). It consists of a pump and two fluid diodes. The diodes are composed of independent thin-film layers and functioned as cantilever diodes. When the pump is pushed, the liquid flows out toward the outlet. However, the liquid does not flow toward the inlet when the pump is released. This allows the liquid to be transported in a single direction by pushing and releasing the pump.

The infused hydrogen peroxide was decomposed into oxygen by using manganese dioxide as the catalyst. The chemical reaction chamber contained manganese dioxide (Figure 2C).

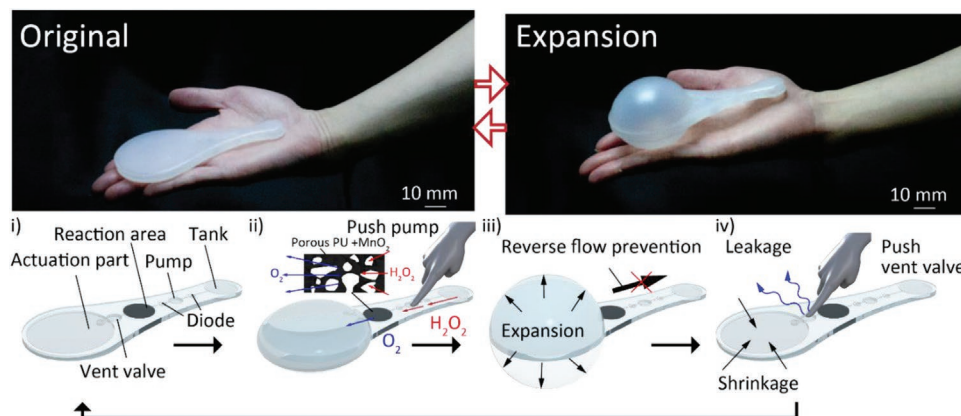


Figure 1. Electric powerless soft actuator based on gas–liquid decomposition reaction. The device functions as an actuator that does not require any external electric power or pumps. The device is driven by four steps: pumping hydrogen peroxide solution with a finger pump, generating gas through a catalytic reaction, driving a balloon-type actuator with the generated gas, and returning to its initial state by operating a vent valve.

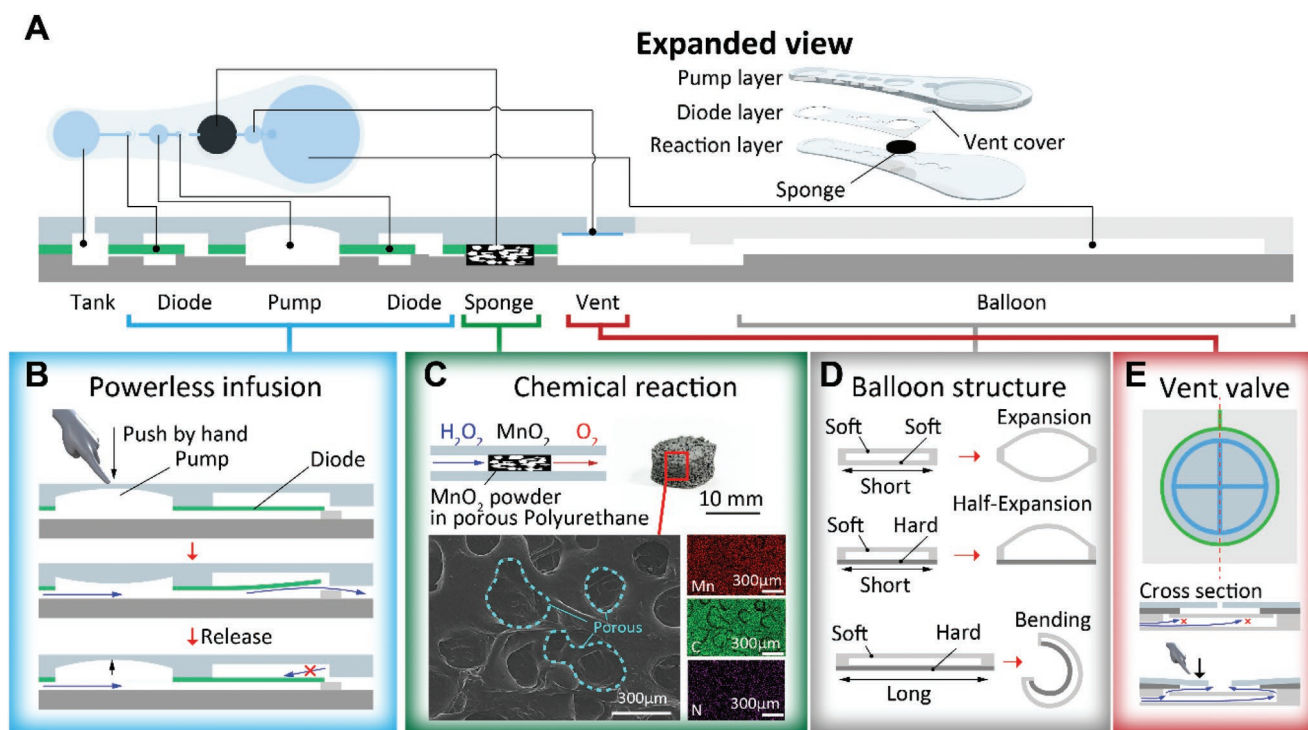


Figure 2. System and mechanism of electric powerless soft actuator. A) Top view, cross section, and expanded view of the device. B–E) The main four functions of the device: manual infusion of hydrogen peroxide, decomposition of hydrogen peroxide, balloon inflation by generated oxygen, and gas leakage. B) Powerless infusion system, consisting of a finger pump and diodes, in which liquid can be transported by driving the pump with the fingers. C) Chemical reaction chamber: the infused hydrogen peroxide solution is decomposed into oxygen by manganese dioxide. D) Balloon actuator: the generated oxygen flows into a balloon made of sealed silicone resin and inflates it. The shape and material of the balloon can be optimized to achieve the desired inflation characteristics. E) Vent valve: the valve maintains the airtightness of the balloon, and can release the gas by applying pressure with a finger. This allows the balloon actuator to inflate and deflate freely and repeatedly.

To increase the efficiency of the reaction between manganese dioxide and hydrogen peroxide, manganese dioxide was infiltrated into the porous polyurethane resin. This allows the hydrogen peroxide solution to contact the manganese dioxide over a larger area and decompose it in a reaction with a high efficiency.

The oxygen generated by the chemical reaction expands the balloon actuator (Figure 2D). Any desired actuator characteristics can be obtained by optimizing the balloon structure and material. After expanding the balloon, oxygen can leak by releasing the vent valve. Thus, the actuator can be returned to its initial state (Figure 2E). This valve has the ability to withstand the internal pressure of the balloon, maintain the expanded shape, and can be deformed by the fingers to leak the gas.

2.1. Properties of the Device

2.1.1. Powerless Infusion System

Figure 3A–C shows the pump characteristics. When the pump diameter was changed, the relationship between the pushing depth and pushing force was investigated, and the pushing depth and output pressure were investigated (Figure 3A). An object with a diameter of 12 mm was used for the pushing motion. Figure 3B shows the relationship between the pushing

force and pushing depth. The graph shows that the pushing force decreases as the pump diameter increases. Figure 3C shows how the output pressure varies with the pushing depth. As shown in the graph, the output pressure increases as the pump was pushed deeper. In contrast, a pump with a diameter of 12 mm yielded the maximum output pressure. The peak diameter depends on the diameter of the object that pushes the pump (Figure S2, Supporting Information). In both cases, the maximum output pressure was less than 2.5 kPa. The diode characteristics are shown in Figure S3 (Supporting Information). The graph shows that the fluid diode fabricated in this study can block reverse flow up to ≈ 20 kPa. This indicates that a diode can be used to ensure the infusion function of the pump.

Several electrically driven micropumps have been studied, including a peristaltic micropump with a piezoelectric element,^[18] and a micropump with microcomponents that rotates using laser irradiation.^[19] These micropumps can be formed on very fine flow paths, and have high-flow-rate resolution (on the nanoliter order) in terms of the infusion volume. However, these electrically driven pumps require external power to drive them. This makes the system more complex and large. Finger pumps were fabricated by integrating the flow path and pump geometry using SU-8 lithography,^[20,21] and the finger pump was mounted on a microfluidic system. While this fabrication method has the advantage of integrating the finger pump into a very fine channel structure by using SU-8 lithography, it is

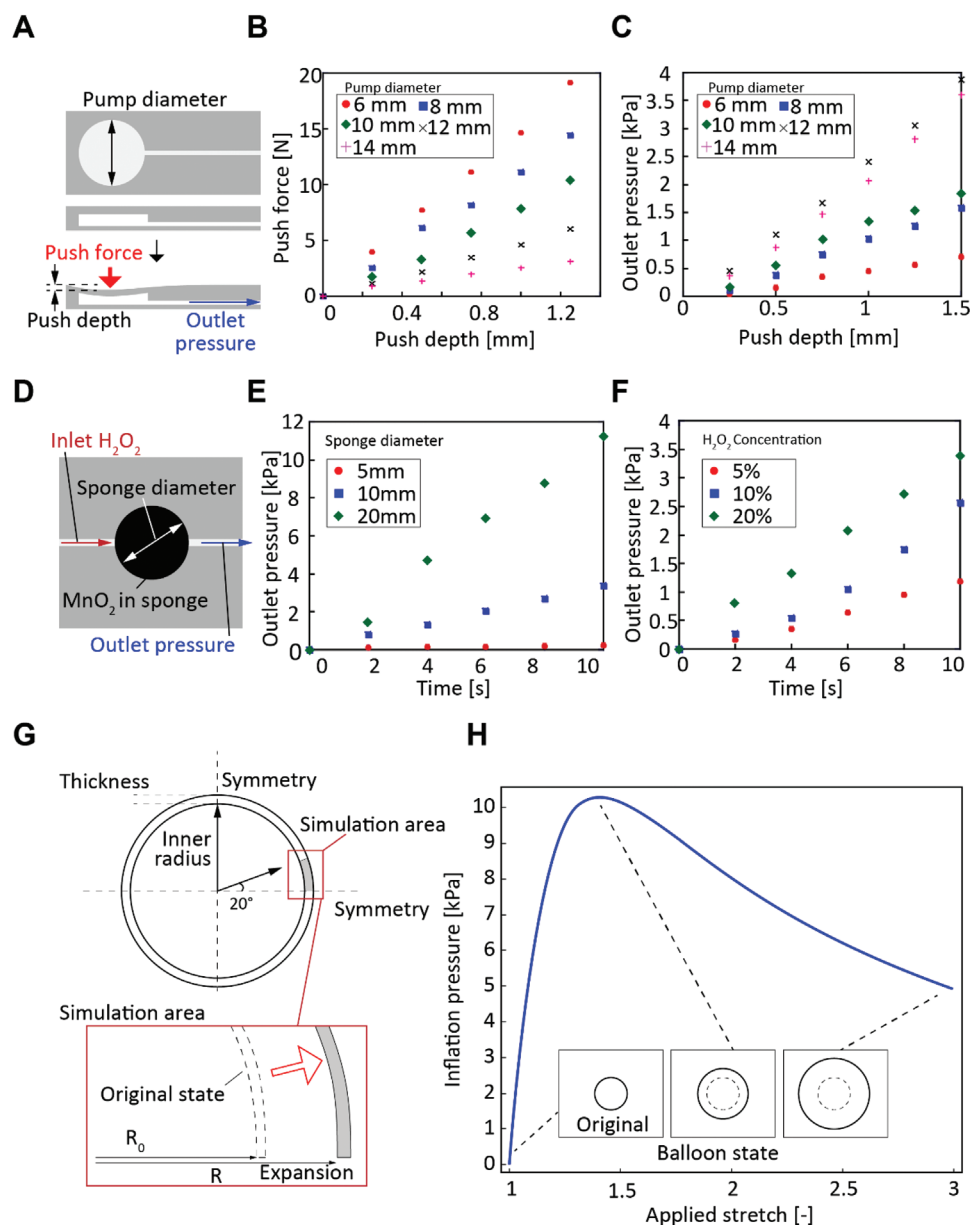


Figure 3. Device characteristics. A) Measured pump performance. Pump diameter, push-down depth, push-down force, and output pressure were measured and compared. B) Relation between pump push-down depth and push-down force. The force required to push down decreases as pump diameter increases. C) Relation between pump push depth and output pressure. The output pressure increases proportionally as the pump is pushed deeper, while the maximum output pressure is observed at a pump diameter of 12 mm. This is dependent on the diameter of the object used for pushing. D) Measurement of reaction sponge performance. The sponge diameter, hydrogen peroxide concentration, and output pressure were measured. E) Comparison of chemical reaction rate by changing the sponge size; the larger the sponge size, the faster the reaction rate and output pressure will be. F) Comparison of chemical reaction rates at different concentrations of hydrogen peroxide solution. Oxygen generation occurred at a faster rate when highly concentrated hydrogen peroxide solution was used. G) Finite element model (FEM) analysis model of a balloon. The balloon shape was assumed to be a sphere, and part of the sphere was used in the analysis. The balloon was subjected to a specified ratio of expansion, and the internal pressure was analyzed. The balloon was inflated up to three times from the original balloon, and the internal pressure was analyzed. H) FEM analysis results. The graph shows that the balloon's internal pressure peaks at an approximate applied stretch equal to 1.4 times, and then decreases slowly.

difficult to control the desired shape and size (especially height when it is in the order of millimeters) of the pump. Therefore, a method for forming the pump was proposed by using a different processing method.^[22] The pump was fabricated by using a 3D printer, and the flow paths were fabricated using photolithography. This enables the fabrication of pumps in the

order of millimeters to centimeters; however, the flow path and pump are not integrated. This structure poses a problem of adhesion between the pump and flow path, which may affect the efficiency of the infusion.

In this study, the pump was fabricated by using 3D printing technology, and its height, shape, and diameter were controlled

as desired. In addition, the pump and flow channel were molded as one piece because the flow channel was fabricated by 3D printing. As shown in Figure 3A, the output pressure was measured by changing the pump diameter to investigate pump performance. Figure 3B shows that the pump can be pushed deeper with a smaller force when the pump diameter is large. However, Figure 3C shows that there is an optimum value for the pump diameter at which the output pressure is maximized. This is because the pushing object pushes the rubber around the pump simultaneously if the object is too large, thus resulting in inefficient pumping and in the decrease of the output pressure. Therefore, the pump diameter at which the output pressure reached its maximum value varied depending on the diameter of the object, as shown in Figure S2 (Supporting Information). This indicates that it is necessary to optimize the pump diameter according to the user's fingertip size when it is applied as a finger pump. The maximum pump output pressure in this study was ≈ 4 kPa, as shown in Figure 3C, and the pressing pressure was ≈ 5 N, as shown in Figure 3B. The finger pump with the SU-8 droplets^[21] yielded an output pressure of 4 kPa at a push of ≈ 10 N. It can be observed that the pressing and output pressures can be controlled by optimizing the pump shape.

A fluid diode with a flap function was fabricated by using silicone rubber modeling via 3D printing technology because a high-gas backflow prevention effect was required as the balloon expanded. Figure S3 (Supporting Information) shows that the diode in this study could block the backflow of gas at ≈ 20 kPa. However, the total diameter of this diode was ≈ 3 mm, which is much larger than that of the SU-8 diode mentioned above. This is because the accuracy of silicone rubber modeling and alignment is lower than that of SU-8 lithography, and miniaturization of this mechanism is a future challenge.

Fluid diodes rectify the fluid by decreasing fluid resistance in one direction, and by increasing it in the other one. Many fluid diodes have been proposed to rectify microfluids. These can be classified into two main types: those with, and those without driving components. A fluid diode without driving components rectifies the fluid by optimizing the flow path structure.^[23,24] These diodes have the advantages of easy fabrication and high durability because they have no driving components. However, they are limited to fluids that can be rectified because the rectification function is maintained by the properties of the fluid itself. A driving component is indispensable for rectifying a wide variety of fluids. There are two types of driving methods, namely, active and passive. The use of an optical laser as an active rectifier diode,^[25] which cannot only stop the backflow, but can also select multiple flow paths and pump objects through them, has been investigated. However, the system is large because it requires an optical laser as an external device, and the location where it can be used is restricted.

Passive diodes prevent fluid backflow by using a driving component with a flap structure that is driven as the fluid moves. A fluid diode using SU-8 lithography technology^[26,27] and a flap-type microfluidic diode using polydimethylsiloxane (PDMS)^[21,28] have been proposed. A diode equipped with this driving component has a very high-rectification effect, and is capable of rectifying and blocking the backflow of liquids as well as gases. The SU-8 fluid diode^[27] has a gas backflow prevention

effect of ≈ 20 kPa, even though it is a very fine diode with a liquid flow path width which is approximately equal to 300 μm . However, this diode allows a small amount of gas leakage in the reverse direction. In contrast, the PDMS fluid diode^[28] almost completely suppressed backflow at pressures as high as 25 psi (≈ 172 kPa). This is due to the high-adhesion properties of silicone rubbers, such as PDMS. By using these types of materials, a high rectification effect is obtained in exchange for the difficulty of microfabrication.

2.2. Chemical Reaction System

Figure 3D–F shows the characteristics of the chemical reaction. The relationship between time and outlet pressure was investigated when the chemical reaction chamber sponge diameter and hydrogen peroxide concentration were changed (Figure 3D). Figure 3E shows the output pressure variation as the catalyst sponge diameter was varied. As shown in the graph, the reaction rate increases as the sponge diameter increases. Figure 3F shows the relationship between the peroxide solution concentration and output pressure. The reaction efficiency increased as a function of the concentration of hydrogen peroxide solution, thus indicating a higher rate of increase in the output pressure.

In addition, the effect of the sponge hole diameter on the reaction rate was tested (Figure S4, Supporting Information). Sponges with four different hole diameters were prepared: nonporous, average pore diameter 5, 0.5, and 0.2 mm. The graph indicates that the reaction rate increases as the hole diameter decreases until 0.5 mm. This is because the increase in the contact between hydrogen peroxide and manganese-dioxide powder as the hole diameter decreases. However, when the average porous diameter is 0.2 mm, the manganese-dioxide powder blocks the pores of the sponge and the liquid cannot pass through sufficiently, resulting in a lower reaction efficiency. This indicates that the pore size must be reduced to obtain high reaction efficiency, but excessive miniaturization of the sponge pores affects the injection of the liquid in the device and reduces the reaction efficiency.

One of the larger demonstration balloon devices in this study required ≈ 10 mL of gas to drive the balloon. As it is difficult to transport this gas by using only a finger pump, this study used a gas–liquid decomposition reaction that can generate a large amount of output with a small amount of liquid infusion. The gas generation reaction is expressed by the following equation



This reaction is a catalytic reaction, and the decomposition reaction occurs when a hydrogen peroxide solution and a catalyst come into contact. Assuming that 1 mL of 10% hydrogen peroxide was completely decomposed, ≈ 600 mL of oxygen was generated in standard conditions. Therefore, several studies have been conducted on driving actuators powered by catalytic reactions of hydrogen peroxide decomposition. Platinum^[29] and catalase^[30] were used as catalysts to decompose a hydrogen peroxide solution to obtain oxygen. Platinum is a metal with

high-chemical and physical stability, but it is also very expensive. Catalase has high biocompatibility, but is prone to degradation over time.

Based on these factors, manganese dioxide was used as the catalyst for decomposition of hydrogen peroxide in this study. The efficiency of the reaction between manganese dioxide and hydrogen peroxide depends on the contact area between the solid and liquid. The reaction efficiency was higher when manganese dioxide was in powder form than when it was in solid form. However, it is difficult to maintain the powder in the device and contact the liquid. In this study, as shown in Figure 2C, urethane resin was formed into a porous structure and coated with manganese dioxide powder to ensure the contact area between hydrogen peroxide and manganese dioxide powder. The porous structure was fabricated by using urethane resin because silicone resin has low wettability,^[31] thus making it difficult to adhere the powder onto the silicone surface. As shown in Figure 2C, manganese particles adhere to the surface of the porous urethane resin. Granulated sugar was used to form a porous structure with an average particle size of $\approx 500 \mu\text{m}$. Although there are other types of sugar, such as caster sugar with smaller particle sizes, sugar with larger particle sizes was used in this study to avoid disturbing the fluid flow.

In addition to the use of porous urethane and manganese dioxide powder to increase reaction efficiency, the size of porous urethane also affects reaction efficiency. As shown in Figure 3E, the reaction rate increases at increasing sponge diameters owing to the increased contact area between the hydrogen peroxide solution and manganese dioxide. If higher reaction efficiency is required, it is necessary to form a porous structure. The reaction efficiency is also affected by the concentration of hydrogen peroxide, as shown in Figure 3F. The rate of decomposition reaction increased as the concentration of hydrogen peroxide increased. Therefore, it is necessary to use a high concentration of hydrogen peroxide to achieve faster reaction; yet, a high concentration of hydrogen peroxide exceeding 10% may have adverse effects on the human body. The concentration must be selected according to the intended use.

2.3. Balloon Expansion Analysis

Finally, the expansion of the balloon section was analyzed by using a finite element method. The balloon shape was assumed to be spherical, and part of the balloon was analyzed (Figure 3G). The analysis was performed by applying a constant magnification to the balloon and calculating its internal pressure at that time. As shown in Figure 3H, the internal pressure peaked at ≈ 1.4 times the initial value, and slowly decreased subsequently.

As shown in Figure 3H, the internal pressure of the balloon increases owing to inflation, and then slowly decreases after reaching the peak. We assumed a rubber of uniform density and thickness, and its spring constant was k . Assuming that the rubber obeys Hooke's law, the tension force on the spring is expressed as $F = kx$ when the rubber is stretched by x from the initial state.

We considered herein a spherical balloon of initial radius r_0 expanded to radius r . For a band with an angle $\Delta\theta$ from the

center of the sphere, this band extends from its original length of πr_0 to a length of πr along the sphere. The tension F applied to this band at this time can be calculated by using the dimensionless constant A as follows

$$F = Ak(r - r_0)\Delta\theta \quad (2)$$

This balloon was inflated from radius r to $r + \delta r$ by considering the equilibrium of the work done by the rubber and the atmospheric pressure inside the balloon. If P_{in} is the air pressure inside the balloon at balloon radius r , and P_0 is the atmospheric pressure, we define P_r as $P_{\text{in}} - P_0$. W_p is the work done by the air inside the balloon against the rubber, expressed as

$$W_p = P_r \frac{4}{3} \pi \{ (r + \Delta r)^3 - r^3 \} \approx 4\pi r^2 \Delta r P_r \quad (3)$$

W_b is the work done by the rubber band at prospective angle $\delta\theta$ expressed as follows

$$\Delta W_b = Ak(\pi r - \pi r_0) \frac{\Delta\theta}{2\pi} \pi \Delta r = \frac{A\pi k}{2} (r - r_0) \Delta r \Delta\theta \quad (4)$$

Integrating this over $0 - 2\pi$ gives the total work done by the rubber

$$W_b = \int_0^{2\pi} \frac{A\pi k}{2} (r - r_0) \Delta r d\theta = A\pi^2 k (r - r_0) \Delta r \quad (5)$$

$$\text{If } W_p = W_b$$

$$4\pi r^2 \Delta r P_r = A\pi^2 k (r - r_0) \Delta r \quad (6)$$

$$\therefore P_r = \frac{A\pi k}{4} \frac{r - r_0}{r^2} = \frac{A\pi k}{4} \frac{1}{r} \left(1 - \frac{r_0}{r} \right) \quad (7)$$

This is proportional to the following values when r approaches the initial radius (r_0)

$$-r_0 \left(\frac{1}{r} - \frac{1}{2r_0} \right)^2 + \frac{1}{4r_0} \quad (8)$$

It is inversely proportional to r when r is sufficiently larger than r_0 . This indicates that the internal pressure of the balloon increases rapidly as a function of radius r to a maximum value in the range close to the initial radius; it then decreases gradually in inverse proportion to the radius in the range where r is greater than r_0 . However, this discussion is limited to the expansion range where Hooke's law can be applied to the elasticity of rubber. The rubber tension increased rapidly when the expansion was extreme at the point of rupture.

To compare the simulation results with the actual deformation, a device with design similar to that designed by the FEM simulation was fabricated and tested (Figure S5, Supporting Information). As shown in the graph, the actual balloon system exhibits a rapid increase in the internal pressure in the early stages of expansion and the pressure begins to decrease at ≈ 1.5 times the rate of expansion. However, the pressure drop

with increasing expansion rate in the actual test results was insufficient compared to the simulation results and the maximum pressure was lower than that in the simulation results. This can be attributed to the difference in shape between the balloon designed for the simulation and the actual device. The balloon designed for the simulation was assumed to be perfectly spherical both before and after inflation, and the film thickness was assumed to be constant. The actual device is made of two hemispherical shells bonded together; thus, the film thickness at the bonded area is different from those at the other areas. This difference in film thickness causes shape changes during expansion. This caused shape and thickness changes during expansion. The maximum pressure was lower than that in the simulation, and the subsequent pressure drop was slower than that in the simulation. Because of these characteristics of balloons, if one part of the balloon is rapidly inflated, the tension in the inflated part is reduced, and the gas will not flow into the other parts of the balloon. Optimization of the structure is required uniform inflation of the balloon.

In addition, the airtightness of the balloon was measured (Figure S6, Supporting Information). The balloon was filled with air and left inflated for 24 h, and the change in internal pressure was measured. The graph indicates that the internal pressure drops to about half in 24 h. This can be attributed to the porous structure of Ecoflex, which has many holes on its surface and is highly gas permeable.^[32] This causes the gas to leak out gradually, resulting in a decrease in the internal pressure. This could be solved by using a less gas permeable resin

such as polyurethane, but polyurethane resins are generally inferior to silicone resins in terms of processability. Therefore, it is more difficult to fabricate complex functional systems such as microfluidic channels and diodes. A simpler solution is to coat the surface with a substance having low gas permeability, such as a liquid metal or fluororesin film.

2.4. Tentacle Gripper Demonstration

A tentacle-shaped gripper device was fabricated by using an actuator device (Figure 4A; and Video S2, Supporting Information). The actuator part of this device was lengthened in a straight line, and resins with different hardness values were used for the upper and lower surfaces (Figure 4B). As shown in Figure 4C, a reaction occurs when a hydrogen peroxide solution is supplied by a finger pump, and the generated oxygen expands and bends the balloon.

In addition, a measurement test was conducted to determine the bending angle of the tentacle in response to an increase in internal pressure (Figure S7, Supporting Information). It can be observed in the graphs that all the tentacle-type actuators bend exponentially as the internal pressure increases. This can be attributed to the fact that the internal pressure to expand the balloon decreases after a certain rate of expansion, as shown in Figure 3; and Figure S5 (Supporting Information). Therefore, we assumed that, once a certain expansion angle is exceeded, the required pressure to expand the balloon becomes less and a slight increase in internal pressure causes a large deformation.

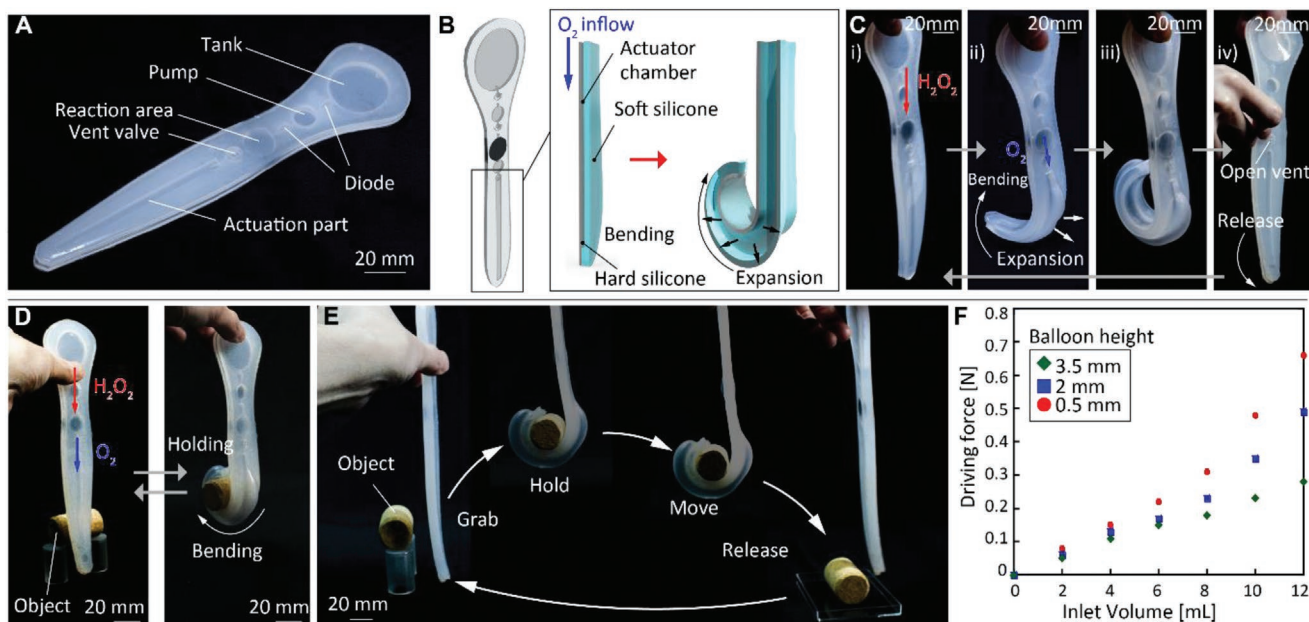


Figure 4. Tentacle gripper device demonstration. A) Photograph of device. B) Computer graphic of tentacle device in operation. The balloon (made of two resins with different hardness) expands and bends in an arc when gas flows into the balloon. C) Photograph of device in operation. The inflow of hydrogen peroxide solution causes a chemical reaction that produces oxygen. The generated oxygen expands the balloon and bends the tip of the device. The device returns to its initial state by releasing the vent valve with a finger. D) Grasping an object with a tentacle device. The tip of the device deforms to wrap around the cylindrical object and grasped it. E) Grasping, moving, and releasing an object with a tentacle device. The tentacle device is used to grasp a cork cylinder, moves it to an arbitrary position, and then, opens again by releasing a valve. F) Comparison of driving force of the tentacle device when the gap height inside the balloon is changed. The driving force is proportional to the volume of inflowing gas; the higher the gap height is, the weaker the driving force will be.

Comparing the data for different space heights inside the balloon, it can be observed that the higher the space height, the greater bending is obtained at a lower pressure. Furthermore, the lower the space height, the greater is the internal pressure required for bending. However, as shown in Figure 4F, the output of the actuator is greater at lower space heights. This indicates that the balloon shape can be designed according to the required bending angle and output.

By opening the valve, the bent balloon returned to its initial state, and the same operation could be repeated several times (Figure S8, Supporting Information). In this experiment, liquid metal was applied to the inflating surface of a balloon, and the state of balloon inflation was measured by measuring the change in the electrical resistance of the liquid metal wiring as the balloon expands and contracts. Because only one side of the actuator inflates when it is inflated, the balloon's inflation state can be measured by reading the deformation of the balloon surface on the side that is inflated. The graph shows that the balloon of the device can expand and contract stably multiple times.

As shown in Figure 4C, the tentacle-type actuator was bent into an almost complete circle via balloon expansion. Similar balloon-shaped bending actuators have been proposed in the past, i.e., a pneumatic bending soft actuator^[33,34] and a bending soft actuator by voltage infusion.^[35] While these actuators use a single material and enable bending motion by optimizing the structure, the tentacle-type actuator fabricated in this study uses a simple band shape as the balloon shape, and instead uses a hard material at the bottom to enable bending motion (Figure 4B). It has also been reported that the shape of the balloon can be arbitrarily deformed by controlling the hardness of the material used at the bottom part.^[36] Furthermore, as shown in Video S2 (Supporting Information), this tentacle, soft robot device can be driven underwater because it is realized without electric power.

Figure 4D shows the grasping of a cylindrical object by using this device. The balloon at the tip of the device was bent by the generated oxygen, and the object could be held and lifted. In addition, the tentacle grippers were used to grasp a rectangular melamine sponge, plastic chess piece (knight), and table-tennis ball (Figure S9, Supporting Information). This device can grasp objects of various shapes, such as squares, cylinders, and spheres. However, a shot glass weighing ≈ 80 g could not be grasped using this device. To grasp heavier objects, the size and material of the device must be optimized.

Figure 4E shows how the object is grasped and moved to an arbitrary position by using this device. By releasing the valve, the balloon returns to a straight shape and the object can be released again. The driving force of the device was measured by using the method as illustrated in Figure S10 (Supporting Information). The bending force of the actuator was measured by using a force gauge with respect to the height of the space inside the balloon. The graph shows that the bending force increased as a function of the height of the space inside the balloon, and that the bending force was proportional to the volume of gas which flowed into the balloon (Figure 4F).

As shown in Figure 4F, the actuator generates a weak force equal to <1 N, while the conventional balloon actuator succeeded in lifting an object which weighed 1 kg.^[37] These results

indicate that balloon actuators can be optimized arbitrarily in terms of driving force, depending on the material and structure. Figure 4F; and Figure S5 (Supporting Information) shows that the height of the internal space of the tentacle balloon affects the driving force of the actuator. The higher the spatial height of the balloon is, the thinner the film thickness at the top of the balloon will be. Balloons composed of thin membranes can be easily bent at lower internal pressures, and the driving force becomes weaker. This indicates that a strong driving force of the actuator can be obtained when the balloon height is low and the top surface of the device is thick.

However, the thickness of the top surface of the balloon is limited. The limit depends on the diode and vent valve functions, as well as on the adhesive ability between the membranes of the device. If the applied pressure exceeds the backflow prevention function of the diode or vent valve, it will break, and gas will leak. The functionality of both the diode and valve was verified with an upper limit of 20 kPa; if a device is fabricated that requires an internal pressure exceeding this limit, it may malfunction. Another limitation is the adhesion between device membranes. The device consisted of three layers, and each of them was bonded by using Ecoflex 00–30. As the balloon expands, these membranes are subjected to forces in the direction of separation, and the adhesion between membranes can be damaged if the internal pressure of the balloon increases excessively. Therefore, the device structure must be optimized to satisfy these requirements.

2.5. Gripper Supporting Device

Based on this mechanism, we demonstrate the implementation of a device that can be attached to the fingertip to assist the user's hand movement (Figure 5A; and Video S3, Supporting Information). This device has an independent balloon actuator and infusion/reaction parts, and can be attached to the fingertip, as shown in Figure 5B. The operating principle is shown in Figure 5C. Driving the pump with the fingertip causes infusion of hydrogen peroxide solution, which is decomposed to oxygen in the chemical reaction chamber on the wrist. Subsequently, the generated oxygen flows into the balloon actuator on the fingertip and expands to grasp an object. This allows users with limited fingertip movements owing to disabilities to assist their finger movements. The device was equipped with two liquid flow channels and reaction chambers, and each of them could be controlled independently.

The actual operation is illustrated in Figure 5D. The balloon was expanded by driving the pump, and the actuator was driven to fill the gap between the fingertips. This makes it possible to grasp objects. Releasing the vent valve causes the balloon to shrink, thus allowing the user to release the grasped object. As shown in Figure S11 (Supporting Information), the actuator expanded and contracted repeatedly and stably.

As shown in Figures S8 and S11 (Supporting Information), the actuator can be repeatedly driven ≈ 10 times. However, after 10 times, the balloon material undergoes plastic deformation and does not fully inflate with the same amount of gas generation as initially. Table S1 (Supporting Information)

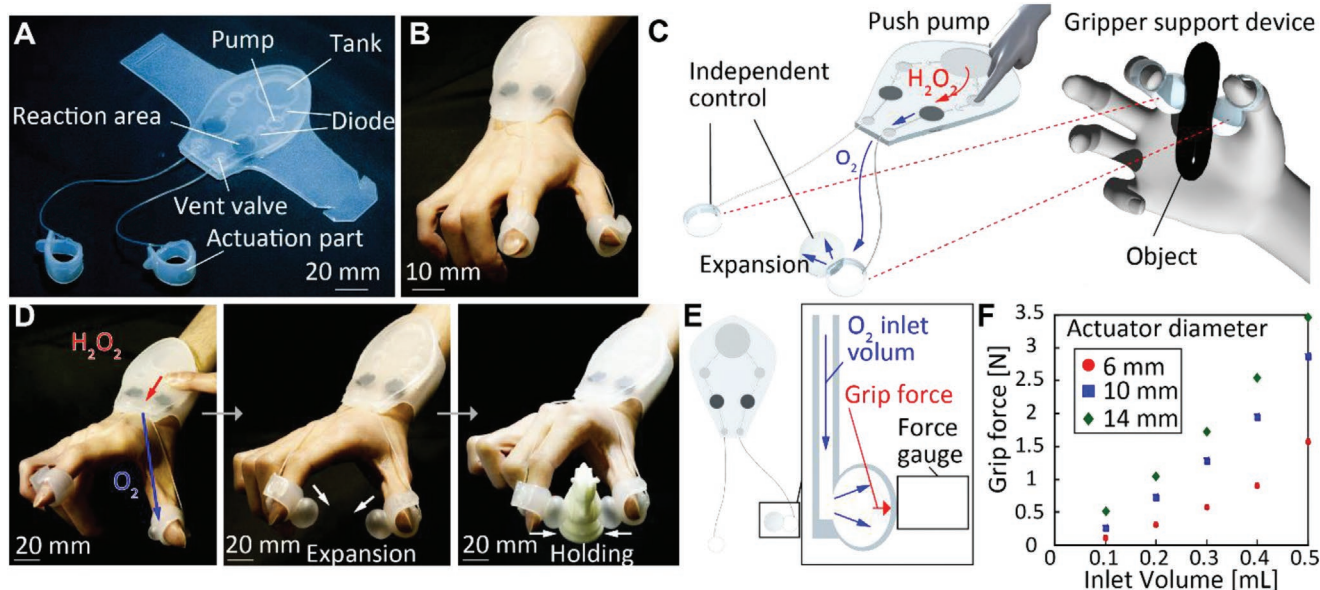


Figure 5. Gripper assisting device. A) Overview of device. B) Photographs of device attached on the wrist and fingers. C) CG image of device in operation. The hydrogen peroxide solution flows into the device when the pump is activated. The hydrogen peroxide is decomposed into oxygen based on a chemical reaction, and the generated oxygen expands the balloons at the fingertips to assist in grasping objects. Two balloons are used, and each of them can be controlled independently. D) Photograph of actuation state. The oxygen generated by a chemical reaction expands the balloons at the fingertips and assists object grasping. E) Gripping force measurement method. The gripping force was measured by using a force gauge. F) Relation between balloon size and gripping force. The gripping force of the gripper increased in proportion to the inflowing gas volume; the larger the balloon diameter is, the stronger the gripping force will be.

shows that Ecoflex 00–30 underwent plastic deformation of $\approx 7.5\%$ after one extension. This causes the deteriorated cycle stability. In contrast, Ecoflex 00–50 exhibited less plastic deformation. However, Ecoflex 00–50 is harder than 00–30; the force required during extension is greater and may damage hermetically sealed parts, such as diodes. Therefore, to improve cycle stability, it is conceivable to optimize the structure to maintain higher hermeticity and backflow prevention, and then fabricate it with a hard resin that is less susceptible to plastic deformation.

The gripping force of the gripper was measured, as shown in Figure 5E. The gripping force was defined as the force that the balloon tip pushes against the object when the balloon was expanded, and was measured by a force gauge (Figure 5F). When the volume of gas which flowed into the balloon was increased, the balloon pushed the object strongly, and the gripping force increased as the balloon diameter increased.

In addition, the repulsive force of the balloon was measured by applying pressure from the top surface during balloon inflation (Figure S12, Supporting Information). As shown in the graph, the larger the diameter of the balloon, the greater is the repulsive force when pushed into the balloon to the same depth. From Figure 5F, it can be observed that the size of the balloon at the gripper tip affects the force to grasp the object. The larger the balloon, the stronger is the grasping force. However, the smaller balloon is suitable for grasping small and flexible objects because it has less repulsive force. Therefore, the shape of the balloon can be optimized according to the object to be grasped, and the wearable actuator can be designed according to the purpose.

The larger balloon requires more gas generation to expand. The gas generation rate can be controlled by adjusting the sponge size, hydrogen-peroxide concentration, and pore diameter, as shown in Figure 3E,F; and Figure S4 (Supporting Information); a large balloon can be efficiently driven by optimizing them. In addition, this device is designed to be used with fingers, and attachment of a balloon device that is much larger than the human fingertip may impair the user's operability. Therefore, the balloon size at the tip of the device needs to be optimized based on the physical characteristics of the object to be grasped and the size of the user's fingers.

As shown in Figure 5, a gripper-assisted device has already been proposed that uses air pressure to inject air and inflate balloons.^[38] The device uses an air pump to inflate the balloon, and has excellent characteristics in terms of both the response speed and object grasping force. However, this device requires hard electronic substrates and pumps on the arm, and an external power supply is required to drive these components. The device fabricated in this study does not require a power supply, and is constructed entirely of soft materials. This can reduce discomfort considerably when applied as a wearable device.

The grasping force of the device shown in Figure 5F indicates that the larger the balloon attached to the fingertip is, the stronger the grasping force will be. This should be optimized by considering both the user's finger size and required grasping force. The grasping force obtained with the 10 mm diameter balloon was ≈ 3 N at an inflow of 0.5 mL of gas; this was sufficient to grasp and lift a chess piece which weighed ≈ 5 g, as shown in Figure 5D. In addition, as shown in Video S3

(Supporting Information), the device successfully grasped and lifted a glass with a flat surface which weighed ≈ 80 g. This is because the balloon material Ecoflex 00–30 generates high friction.

To test the friction of the Ecoflex gripper, a portion (10×25 mm²) of the Ecoflex 00–30 was attached to several flat surfaces with different surface roughnesses, and the force required to pull it off horizontally was measured using a force gauge (Figure S13, Supporting Information). As shown in the graph, the gripping force decreases for objects with rough surfaces. Objects with smooth surfaces require a force of ≈ 0.5 N to peel off. Because the material can be flexibly deformed and fits the object's shape, the gripper can firmly grip the object. It also successfully grasped and lifted a flexible sponge which weighed ≈ 0.5 g without deforming it. This indicates that the device can grasp objects gently. This is because the gripping part of the device is made of flexible material that can be deformed to fit the object.

However, this device has a drawback in that the balloon material is fragile. Depending on the shape and mass of the object to be grasped, the balloon may tear and cease functioning. Currently, the objects that can be grasped are flat glass and plastic; the device is still not suitable for grasping sharp and heavy metals. Another issue is the response time; it took ≈ 15 s from the initial state to the fully inflated and grasped state. This response time can be improved by optimizing the pore size and structure of the chemical reaction chamber to increase the decomposition efficiency of hydrogen peroxide and increase the concentration of hydrogen peroxide, while ensuring the airtightness and safety of the device itself. In this study, a hydrogen peroxide solution with a concentration of 7% was used for safety reasons. High concentrations of hydrogen peroxide (30% or more) are dangerous because they oxidize the skin surface when they adhere to the skin. It would be possible to use highly concentrated hydrogen peroxide by introducing a structure that can prevent liquid leakage from the device with high precision. Because the concentration of hydrogen peroxide affects the reaction rate, optimization of other parts that affect reaction efficiency, such as the size of the reaction chamber and the diameter of the porous holes, is also necessary to maintain reaction efficiency when using a low-concentration solution.

3. Conclusion

In this study, four mechanisms were used: an infusion system that used a finger pump and a fluid diode without electricity, decomposition of liquid to generate gas by a chemical reaction chamber, driving of a balloon actuator by using the generated gas, and return to the initial state by using a vent valve. The actuator was designed to generate an output without external electrical power. The actuator can be applied to soft robots and wearable devices to assist people with disabilities. In comparison to conventional power-driven soft robots, the actuator is a simple system that can be driven as a stand-alone device. The actuator does not require a pump or power source, and all components, including the driving parts, can be made of soft materials. The concept of a battery-less actuator will also contribute to the future development of soft robots and wearable devices in terms of portability and convenience.

4. Experimental Section

The fabricated device was composed of two types of silicone resins with different hardness values. The mechanical part that performed the infusion and reaction was made of hard silicone to prevent deformation. The driving part that functions as a balloon actuator was made of simple Ecoflex 00–30, which is softer than the others. In addition, this device consisted of three layers, and an organic solvent solution of silicone resin was used to adhere to each layer. The material was then sprayed onto each layer. For the part where the chemical reaction occurred, a porous polyurethane resin was used to increase reaction efficiency. The reaction was performed by infiltrating a water dispersion of manganese dioxide into the porous resin.

A harder silicone resin was prepared by mixing KE-1603 and Ecoflex 00–30. First, 10 g of KE-1603 (Shin-Etsu silicone) were mixed with 1 g of curing agent. Subsequently, 5 g of Ecoflex 00–30 Agent A and 5 g of Agent B were added and mixed together. Thus, a silicone resin harder than the simple Ecoflex 00–30 was obtained (hereafter referred to as KE-Ecoflex mixed resin). Spray adhesion was prepared by mixing 5 g of Ecoflex 00–30 A and 5 g of B and dissolving in 10 mL of hexane.

Figure S14 (Supporting Information) shows the fabrication method implemented in the porous urethane chemical reaction chamber. First, a mold was fabricated by using a 3D printer, and was filled with granulated sugar (Figure S14i, Supporting Information). Subsequently, a mixture of Gummy Cast (Craft Resin) A (5 g) and B (3 g) was injected from the top surface, vacuumed to 0.8 MPa for 5 min, and then cured at 70 °C for 30 min (Figure S14ii, Supporting Information). After curing, the resin was placed in distilled water and sonicated for 2 h to remove the granulated sugar and obtain a porous polyurethane resin (Figure S14iii, Supporting Information). After peeling it from the mold, the sponge sheet was cut to a diameter of 10 mm by using a punch (Figure S14iv, Supporting Information). Water dispersion of manganese dioxide powder was used as the catalyst for the chemical reaction. Manganese dioxide powder (4 g) was added to 10 mL of distilled water and dispersed in an ultrasonic bath for 10 min to obtain manganese dioxide dispersion. The reaction sponge was prepared by infiltrating it with manganese dioxide water dispersion and drying it at 70 °C for 60 min (Figure S14v, Supporting Information).

Figure S15 (Supporting Information) shows the fabrication method for the actuator device. Figure S15i–iii (Supporting Information) shows the fabrication method of the pump layer. First, a pump layer mold was fabricated by the 3D printer, KE-Ecoflex mixed resin was poured into the infusion mechanism area, Ecoflex 00–30 was poured into the balloon actuator area, and was then cured at 70 °C for 30 min (Figure S15i, Supporting Information). Second, the liquid inlet to the tank and vent hole were punched, and a circular sheet of KE-Ecoflex resin was attached to the valve by Sil-poxy (Figure S15ii, Supporting Information). This completed the pumping layer. Subsequently, the valve area was masked with polyimide tape, and the top surface was spray-coated with spray adhesive solution (Figure S15iii, Supporting Information).

Figure S15iv,v (Supporting Information) shows the fabrication method of the diode layer. The diode layer mold was fabricated by using a 3D printer, and the KE-Ecoflex resin mixture was poured into it (Figure S15iv, Supporting Information). The diode layer was obtained by peeling it off from the mold (Figure S15v, Supporting Information). Figure S15vi–ix (Supporting Information) shows the fabrication method of the reaction layer. First, a mold with the reaction layer shape was fabricated by using a 3D printer. KE-Ecoflex mixed resin was poured into the infusion mechanism area, Ecoflex 00–30 was poured into the balloon actuator area, and was then cured at 70 °C for 30 min (Figure S15vi, Supporting Information). Second, the driving part of the diode layer was masked with polyimide tape and the spray adhesive was sprayed onto the surface (Figure S15vii, Supporting Information). Third, the diode layer was attached and cured at 70 °C for 15 min, and the reaction sponge was attached to the reaction layer with Sil-Poxy (Figure S15viii, Supporting Information). Finally, a pump layer coated with spray adhesive solution was attached to the top of these layers and cured at 70 °C for 20 min to fabricate the device (Figure S15ix, Supporting Information).

Supporting Information

Supporting Information is available from the Wiley Online Library or from the author.

Acknowledgements

This work was supported by the Japanese Science and Technology Agency, PRESTO Grant (No. JPMJPR18J2) and JSPS KAKENHI Grant (No. 20H00213).

Conflict of Interest

The authors declare no conflict of interest.

Author Contributions

Conceptualization: H.O., R.M., and Z.S. Investigation: R.M. and Z.S. Visualization: R.M. Supervision: H.O. Writing—original draft: R.M. Writing—review and editing: H.O. and R.M.

Data Availability Statement

The data that support the findings of this study are available from the corresponding author upon reasonable request.

Keywords

catalytic reaction, finger-operated pump, fluidic circuit, soft actuator

Received: September 20, 2022

Revised: October 30, 2022

Published online:

- [1] S. Shigetomi, H. Takahashi, F. Tsumori, *J. Photopolym. Sci. Technol.* **2020**, *33*, 193.
- [2] W. Hu, G. Z. Lum, M. Mastrangeli, M. Sitti, *Nature* **2018**, *554*, 81.
- [3] R. v. Ramanujan, L. L. Lao, *Smart Mater. Struct.* **2006**, *15*, 952.
- [4] K. Matsubara, D. Tachibana, R. Matsuda, H. Onoe, O. Fuchiwaki, H. Ota, *Adv. Intell. Syst.* **2020**, *2*, 2000008.
- [5] K. Nagase, T. Okano, H. Kanazawa, *Nano-Struct. Nano-Objects* **2018**, *16*, 9.
- [6] Y. J. Jin, B. S. il Kim, W. E. Lee, C. L. Lee, H. Kim, K. H. Song, S. Y. Jang, G. Kwak, *NPG Asia Mater.* **2014**, *6*, e137.
- [7] S. Y. Tang, V. Sivan, P. Petersen, W. Zhang, P. D. Morrison, K. Kalantar-zadeh, A. Mitchell, K. Khoshmanesh, *Adv. Funct. Mater.* **2014**, *24*, 5851.
- [8] G. Mao, M. Drack, M. Karami-Mosammam, D. Wirthl, T. Stockinger, R. Schwödäuer, M. Kaltenbrunner, *Sci. Adv.* **2020**, *6*, eabc0251.
- [9] Y. Z. Liu, Z. W. Hao, J. X. Yu, X. R. Zhou, P. S. Lee, Y. Sun, Z. C. Mu, F. L. Zeng, *Smart Mater. Struct.* **2019**, *28*, 055011.
- [10] R. F. Shepherd, F. Ilievski, W. Choi, S. A. Morin, A. A. Stokes, A. D. Mazzeo, X. Chen, M. Wang, G. M. Whitesides, *Proc. Natl. Acad. Sci. USA* **2011**, *108*, 20400.
- [11] T. Sun, Y. Chen, T. Han, C. Jiao, B. Lian, Y. Song, *Robot Comput. Integr. Manuf.* **2020**, *61*, 101848.
- [12] K. Shiota, T. V. J. Tarvainen, M. Sekine, K. Kita, W. Yu, *Advances in Intelligent Systems and Computing*, Springer, Berlin **2017**, pp. 525–537.
- [13] X. Li, C. O. Chui, *Microfluid. Nanofluid.* **2018**, *22*, 14.
- [14] W. Li, T. Chen, Z. Chen, P. Fei, Z. Yu, Y. Pang, Y. Huang, *Lab Chip* **2012**, *12*, 1587.
- [15] Y. Whulanza, T. A. Hakim, M. S. Utomo, R. Irwansyah, J. Charmet, Warjito, *Evergreen* **2019**, *6*, 108.
- [16] Q. Ma, S. Liao, Y. Ma, Y. Chu, Y. Wang, *Adv. Mater.* **2021**, *33*, 2102096.
- [17] M. J. Azevedo, I. Correia, A. Portela, B. Sampaio-Maia, *J. Adv. Prosthodont.* **2019**, *11*, 155.
- [18] T. Ma, S. Sun, B. Li, J. Chu, *Sens Actuators, A* **2019**, *292*, 90.
- [19] S. Maruo, H. Inoue, *Appl. Phys. Lett.* **2006**, *89*, 144101.
- [20] J. Park, J. K. Park, *Anal. Chem.* **2019**, *91*, 11636.
- [21] K. Iwai, K. C. Shih, X. Lin, T. A. Brubaker, R. D. Sochol, L. Lin, *Lab Chip* **2014**, *14*, 3790.
- [22] S. Lee, H. Kim, W. Lee, J. Kim, *Micro Nano Syst. Lett.* **2018**, *6*, 1.
- [23] W. J. Hyun, S. Kumar, L. F. Francis, C. D. Frisbie, *Appl. Phys. Lett.* **2018**, *113*, 193701.
- [24] Z. Liu, W. Q. Shao, Y. Sun, B. H. Sun, *Eng. Appl. Comput. Fluid Mech.* **2022**, *16*, 441.
- [25] R. W. Applegate, J. Squier, T. Vestad, J. Oakey, D. W. M. Marr, P. Bado, M. A. Dugan, A. A. Said, *Lab Chip* **2006**, *6*, 422.
- [26] V. Seidemann, S. Bütetfisch, S. Büttgenbach, *Sens. Actuators, A* **2002**, *97–98*, 457.
- [27] Z. Mao, K. Yoshida, J. wan Kim, *Microsyst. Technol.* **2019**, *25*, 245.
- [28] M. L. Adams, M. L. Johnston, A. Scherer, S. R. Quake, *J. Microelect. Microeng.* **2005**, *15*, 1517.
- [29] M. Wehner, R. L. Truby, D. J. Fitzgerald, B. Mosadegh, G. M. Whitesides, J. A. Lewis, R. J. Wood, *Nature* **2016**, *536*, 451.
- [30] Y. Wakabayashi, T. Okamoto, H. Saito, H. Kudo, K. Mitsubayashi, in *TRANSDUCERS 2007 –2007 International Solid-State Sensors, Actuators and Microsystems Conference*, IEEE, Piscataway, NJ **2007**, p. 2211.
- [31] G. Momen, M. Farzaneh, R. Jafari, *Appl. Surf. Sci.* **2011**, *257*, 6489.
- [32] N. Ochirkhuyag, Y. Nishitai, S. Mizuguchi, Y. Isano, S. Ni, K. Murakami, M. Shimamura, H. Iida, K. Ueno, H. Ota, *ACS Appl. Mater. Interfaces* **2022**, *14*, 48123.
- [33] Z. Xie, A. G. Domel, N. An, C. Green, Z. Gong, T. Wang, E. M. Knubben, J. C. Weaver, K. Bertoldi, L. Wen, *Soft Robot* **2020**, *7*, 639.
- [34] A. Zolfagharian, M. A. P. Mahmud, S. Gharaiea, M. Bodaghi, A. Z. Kouzani, A. Kaynak, *Virtual Phys. Prototyping* **2020**, *15*, 373.
- [35] V. Cacucciolo, J. Shintake, Y. Kuwajima, S. Maeda, D. Floreano, H. Shea, *Nature* **2019**, *572*, 516.
- [36] L. Zheng, S. Yoshida, Y. Morimoto, H. Onoe, S. Takeuchi, in *IEEE International Conference on Micro Electro Mechanical Systems (MEMS)*, IEEE, Piscataway, NJ **2015**, p. 18.
- [37] A. Miriyev, K. Stack, H. Lipson, *Nat. Commun.* **2017**, *8*, 596.
- [38] X. Zhang, V. Michael Bove, V. K. Chen, J. Zeng, A. Shtarbanov, P. Maes, J. Rekimoto, in *Conference on Human Factors in Computing Systems*, Association For Computing Machinery, New York **2019**, pp. 1–6.